ACS APPLIED MATERIALS & INTERFACES

Letter

www.acsami.org

Fabrication of Bimetallic Nanostructures via Aerosol-Assisted Electroless Silver Deposition for Catalytic CO Conversion

Jeong Hoon Byeon*,† and Jang-Woo Kim*,‡

†Department of Chemistry, Purdue University, West Lafayette, Indiana 47907, United States

‡Department of Digital Display Engineering, Hoseo University, Asan 336-795, Republic of Korea

Supporting Information

ABSTRACT: Bimetallic nanostructures were fabricated via aerosol-assisted electroless silver deposition for catalytic CO conversion. An ambient spark discharge was employed to produce nanocatalysts, and the particles were directly deposited on a polytetrafluoroethylene substrate for initiating silver deposition to form Pd–Ag, Pt–Ag, Au–Ag bimetallic nanostructures as well as a pure Ag nanostructure. Kinetics and morphological evolutions in the silver deposition with different nanocatalysts were comparatively studied. The Pt catalyst displayed the highest catalytic activity for electroless silver deposition, followed by the order Pd > Au > Ag. Another catalytic activity of the fabricated bimetallic structures in the carbon monoxide conversion was further evaluated at low-temperature conditions. The bimetallic systems showed significantly higher catalytic activity than that from a pure Ag system.

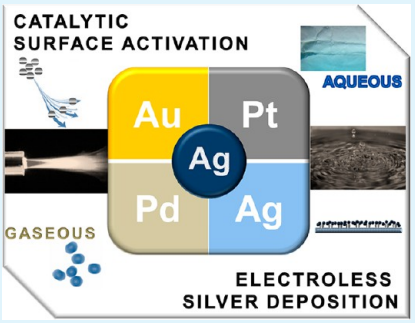

KEYWORDS: *bimetallic nanostructures, aerosol-assisted, electroless silver deposition, carbon monoxide conversion*

INTRODUCTION

Noble metal nanoparticles such as gold (Au), platinum (Pt), and palladium (Pd) nanoparticles have attracted considerable attention because of their exceptional activity as catalysts.[1] Bimetallic nanoparticle systems, in particular, draw higher attention due to their technological and scientific features for improving catalytic properties.[2] Several approaches have been established for fabricating bimetallic structures, including chemical reductions, electrochemical approaches, and vacuum processes. Among these techniques, electroless deposition (ELD) has been regarded as one of the most suitable processes because of its simplicity and low cost.[3−5]

The mechanism underlying ELD involves activation, which is a catalytic reaction triggered by active particles on the surface of substrates dipped into an electroless bath. The active catalyst acts as an electron carrier for the transfer of electrons from the reducing agent to the metal ions. Hence, the structure and composition of the catalyst can alter deposition rates and reaction kinetics.[6] The most commonly used ELD method employs wet tin (Sn)-sensitization and Pd-activation steps. Other activation methods can also be employed, such as ion implantation, spin-coating laser exposure, and dip coating.[7] However, there are still major problems for commercialization, including impurities, complex steps, and environmental pollution from multistep wet chemistry.[8,9] Moreover, it is hard to determine precise catalytic activity in deposition kinetics because of Sn-protected configuration. It would be advantageous to activate the substrate surface through simple, more effective, and more environmentally friendly means.[10] In previous studies, the authors prepared different metal nanoparticles and used them as activators for ELD.[11−14] For electroless reaction, the authors synthesized different noble metal nanocatalysts from ambient spark discharges by replacing precursor electrodes; the nanocatalysts were prepared without the use of Sn-sensitization (as impurities, thus deteriorating catalytic activity),[15] and thus showed an enhanced catalytic activity.

As a significant expansion of the previous reports, this work employs ambient spark discharges of noble metals to assess the kinetics and morphological evolution in electroless silver (Ag) deposition. Most efforts have been devoted to Ag deposition via Pd catalysts with less work being performed on the comparison between noble metals. At the initial stage of electroless Ag deposition, the catalytic particles serve as the anodic site at which the reductant can be adsorbed and oxidized. Formally speaking, the electrons released during oxidation travel through the catalytic particles and reduce ionic Ag. The particles act as electron transfer carriers from the reducing agent to the Ag ions, hence resulting in further deposition (Scheme 1).

Fabrication of catalytic membranes via ELD is a widely used technique to form catalyst layers on porous substrates.[16] Carbon monoxide (CO) is an air pollutants, and catalysts containing noble metals have been extensively studied for their abatement of CO through oxidation processes.[5] In particular, noble metal-based bimetallic catalysts exhibited extraordinary high activity at a relatively low temperature due to their strong adsorption ability of CO molecules.[17] Furthermore, the Ag component facilitated completion of research on the effects of the addition of a second metal to noble metal catalysts on the catalytic performance of CO conversion. This is because the

Received: January 3, 2014
Accepted: February 24, 2014
Published: February 24, 2014

   dx.doi.org/10.1021/am500047n | ACS Appl. Mater. Interfaces 2014, 6, 3105−3110

Scheme 1. Electroless Deposition of Catalytically Activated Polymer Substrates with Different Spark-Produced Metal Particles; Photos of the Activated Substrates Are Also Shown

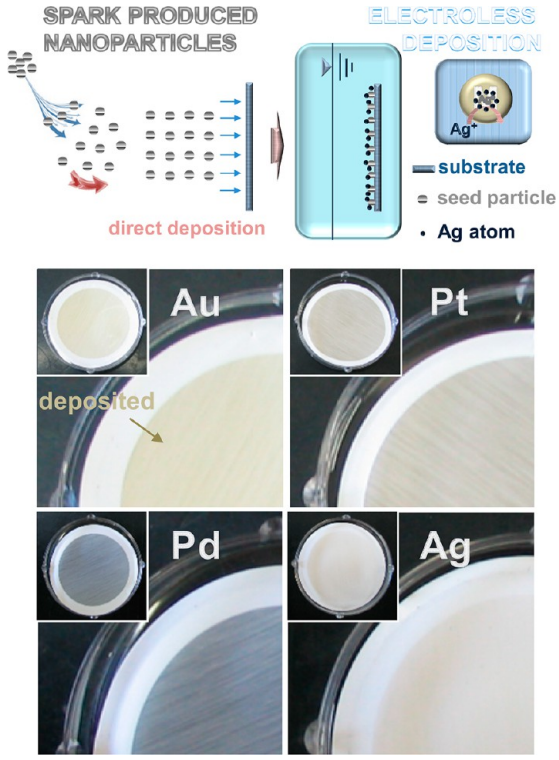

transport of oxygen is no longer a limiting factor because it cannot complicate the kinetic. Hence, in the present work, the fabricated bimetallic nanostructures via electroless Ag deposition on different noble metal nanocatalysts were employed to verify catalytic activity for efficient low temperature CO conversion.

RESULTS AND DISCUSSION

The size distributions of the spark-produced metal particles were measured using a scanning mobility particle sizer (SMPS, 3936, TSI, U.S.), and the results are provided in Figure 1. The total number concentration, geometric mean diameter, and geometric standard deviation of the spark-produced Pd particles are 1.81×10^6 particles cm^{-3}, 40.4 nm, and 1.50, respectively. The same data for the other metal particles are summarized in Table SI in the Supporting Information. The discrepancy with the primary particle size on the transmission electron microscope (TEM, JEM-3010, JEOL, Japan) image (Figure 2a) indicates that the particles agglomerate a few seconds between spark discharge and SMPS measurement. Using coagulation theory, we estimated that the initial primary particle concentration should be closed to the spark between 1×10^9 and 1×10^{10} cm^{-3}.

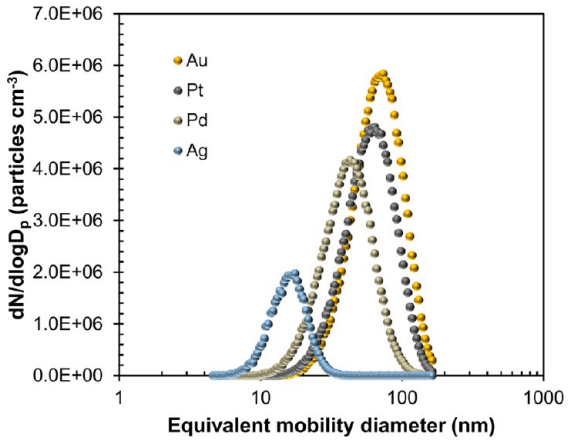

Figure 1. Size distributions of spark-produced Au, Pt, Pd, and Ag particles under N_2 flow environment. Standard deviations are noted in Table SI in the Supporting Information.

The TEM images (Figure 2a) reveal that both the morphologies of the spark-produced particles were agglomerates of several primary particles (each ~3.6 nm in lateral dimension). The TEM image shows larger sizes of the nanoparticles than those measured by SMPS owing to gathering individual nanoparticle during the direct electrostatic aerosol sampling. In high-magnification TEM images, all the fringes have a gap showing the (111) Miller indices of the face-centered cubic (fcc) lattice for metallic Au, Pt, Pd, and Ag, which indicated that all the spark-produced particles grew predominantly along the (111) lattice and mostly consisted of several nanometer size crystallites. A deposition density (D_d) of the substrate with spark-produced nanocatalysts is defined as follows[18]

$$D_d(D_p) = Qt_dA_s^{-1}m^{-1}\int_0^\infty \eta(D_p)C_a(D_p)dD_p \quad (1)$$

where Q is the flow rate of the carrier gas, t_d is the deposition time, A_s is the plane area of the substrate, η (D_p) is the deposition efficiency, and C_a (D_p) is the area concentration of nanocatalysts. The deposition density on a polytetrafluoroethylene (PTFE) substrate was selected to be approximately 1.94×10^{-2} mm^2 of catalyst mm^{-2} of the substrate. Scanning electron microscope (SEM, JSM-6500F, JEOL, Japan) images (see Figure S1 in the Supporting Information) showed that the untreated PTFE substrate had a clean surface, while a number of particles (i.e., nanocatalysts) were deposited on the activated PTFE substrate (Figure 2b). It can be seen that these nanocatalysts are composed of primary particles distributed on substrate surfaces. By looking at the images closely, it is clear that the Ag nanocatalysts are much more uniform than other nanocatalysts, which are probably due to the size difference between Ag and others (16 nm vs 40−66 nm in mobility equivalent diameter) even though spark operation conditions were identical for all of the nanocatalysts. Significant differences in particle concentration (0.6×10^6 particles cm^{-1} vs $1.8-2.6 \times 10^6$ particles cm^{-1} in particle number concentration) may also affect the morphology of nanocatalyst layers. Formation of the web-like networks on the substrates, because of gathering individual agglomerates during the activation, was clearly seen in the Au, Pt, and Pd cases because higher concentrations are commonly favorable for agglomerate between primary particles.

Figure 3 shows SEM and energy-dispersive X-ray (EDX, JED-2300, JEOL, Japan) results of the electroless Ag deposited polymer substrates. As shown in Figure 3a, the Ag deposition occurred on the catalyst particles. The catalyst particles effectively acted as activators to initiate Ag deposition. The process was hence clearly observed to occur by the initial nucleation at several sites on the substrate followed by growth around these nucleated sites.[19] Even though the Ag particles were densely packed on the substrates after 10 min of the Ag deposition, their morphologies were quite different. A report

dx.doi.org/10.1021/am500047n | ACS Appl. Mater. Interfaces 2014, 6, 3105−3110

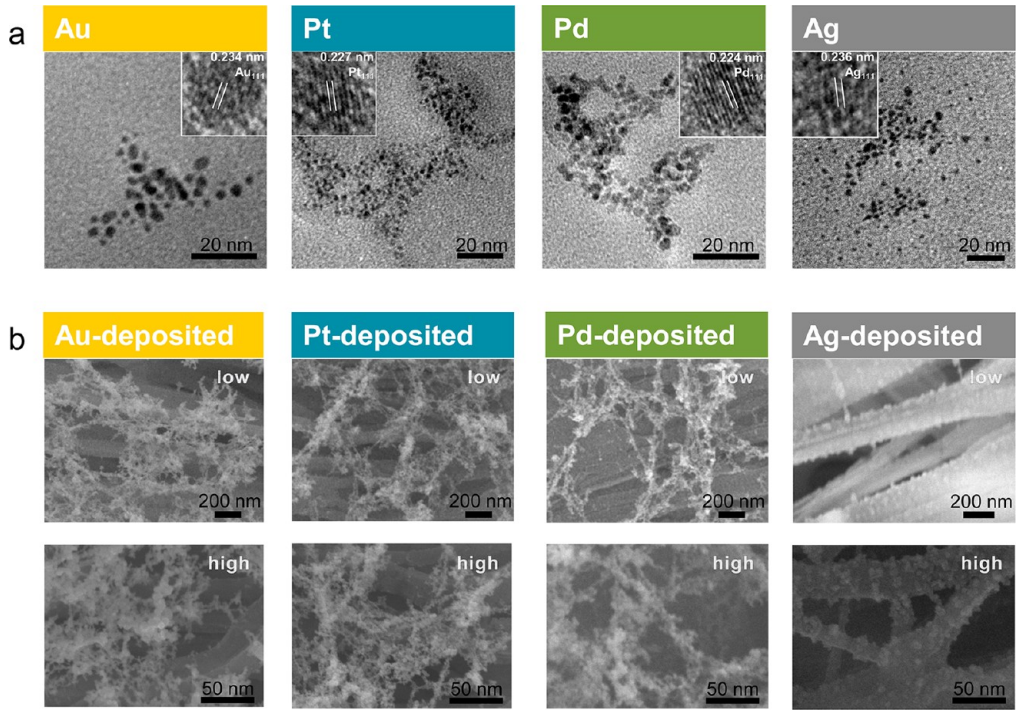

Figure 2. Results of catalytic surface activation using spark-produced metal particles. (a) Low- and high-magnification TEM images of spark-produced Au, Pt, Pd, and Ag particles. (b) Low- and high-magnification SEM images of catalytically activated polymer substrates with the spark-produced particles.

from Byeon and Kim (2010) demonstrated that the morphology of the electroless metal particles was largely influenced by catalyst properties since the nucleation resulted in electroless particles formed directly on top of the catalyst particles (see Scheme S1 in the Supporting Information).[12] In the case of Au nanocatalysts, isolated Ag islands coalesce into near equilibrium compact shapes forming percolating structures. For Pt and Pd nanocatalysts, three distinct stages such as isolated islands, coalesce equilibrium shapes, and continuous deposits during Ag particle growth were clearly observed as they passed through a sequence of morphological changes. In the early stages, isolated islands developed around the nanocatalysts. As the deposition proceeded, they became larger spherical particles but remained compact islands. Such a morphological difference between Au and Pt (or Pd) nanocatalysts in the Ag deposition could be attributed to their lattice parameters (Au = 0.408 nm, Pt = 0.392 nm and Pd = 0.389 nm vs Ag = 0.409 nm). A larger lattice mismatch between Ag and Pt (or Pd) may introduce growth that is significantly larger for Ag islands, whereas Au nanocatalysts with a nearly identical lattice parameter to Ag in crystallinity, resulted in the formation of a flat Ag film. Another difference in electroless Ag size between Pt and Pd nanocatalysts might have originated from different catalytic activities between the nanocatalysts for hydrazine oxidation during Ag ELD. In addition, a morphological difference in nanocatalyst on the substrates might also affect the Ag size. The particle shape of electroless Ag particles deposited on the Ag nanocatalysts resembles the Ag nanocatalysts. The Ag particles deposited on the Ag catalysts surface were also discontinuous, similar to those of Pt and Pd but composed of smaller particles probably because of the scattered distribution of the Ag catalysts. After 10 min of deposition in this experiment, the Ag particles on the spark-produced Ag on the substrate propagated to isotropic growth of the electroless Ag, and thus they had a larger surface coverage than those from Pt and Pd. EDX maps (Figure 3b) correspond to catalysts (Au, Pt, and Pd) and electroless Ag, and the dots in these maps indicate the positions of each element on the substrates. The EDX maps indeed verify that the catalyst particles and electroless Ag coexisted on the substrates. The maps show that both the catalyst and electroless Ag were spread out over the entire surface.

Deposition kinetics could be described as progressive nucleation on nanocatalysts at the initial stage followed by the diffusion of Ag ions toward the growing nucleus islands, and thus the type of catalysts significantly affects the kinetics by providing an alternative reaction path with lower activation energy. According to the inductively coupled spectroscope (Elan 6000, Perkin-Elmer, US) measurements (Figure 4), the Pt catalyts displayed the highest catalytic activity for electroless Ag deposition, followed by the order Pd > Au > Ag, which implies that Ag deposition on Pt catalysts could automatically generate the best catalysis for the ELD to speed up the reaction. This kinetic order is mostly consistent with previous reports where the deposition rates corresponded to their activation energies (see the Supporting Information), i.e., 17 kJ mol^{-1} (Pt), 38 kJ mol^{-1} (Pd), 59 kJ mol^{-1} (Au), and 42 kJ mol^{-1} (Ag) for anodic oxidation of hydrazine, although there is a mismatch between Au and Ag nanocatalysts.[16,20] Nevertheless, the order of deposition kinetics corresponds to the magnitude (Pt > Pd > Au > Ag) of the metal−hydrogen (i.e., catalyst-reductant) bond energy.[21,22] In other words, the higher energy of the metal−hydrogen bond can induce more reductant adsorption being oxidized on the nanocatalysts. In addition, as can be seen in Figure S2 in the Supporting Information, a steady-state reaction potential that is further observed during the ELD is triggered by the different nanocatalysts. The potentials measured for the different Au, Pt, Pd, and Ag catalysts were −0.64, −0.79, −0.70,

dx.doi.org/10.1021/am500047n | ACS Appl. Mater. Interfaces 2014, 6, 3105−3110

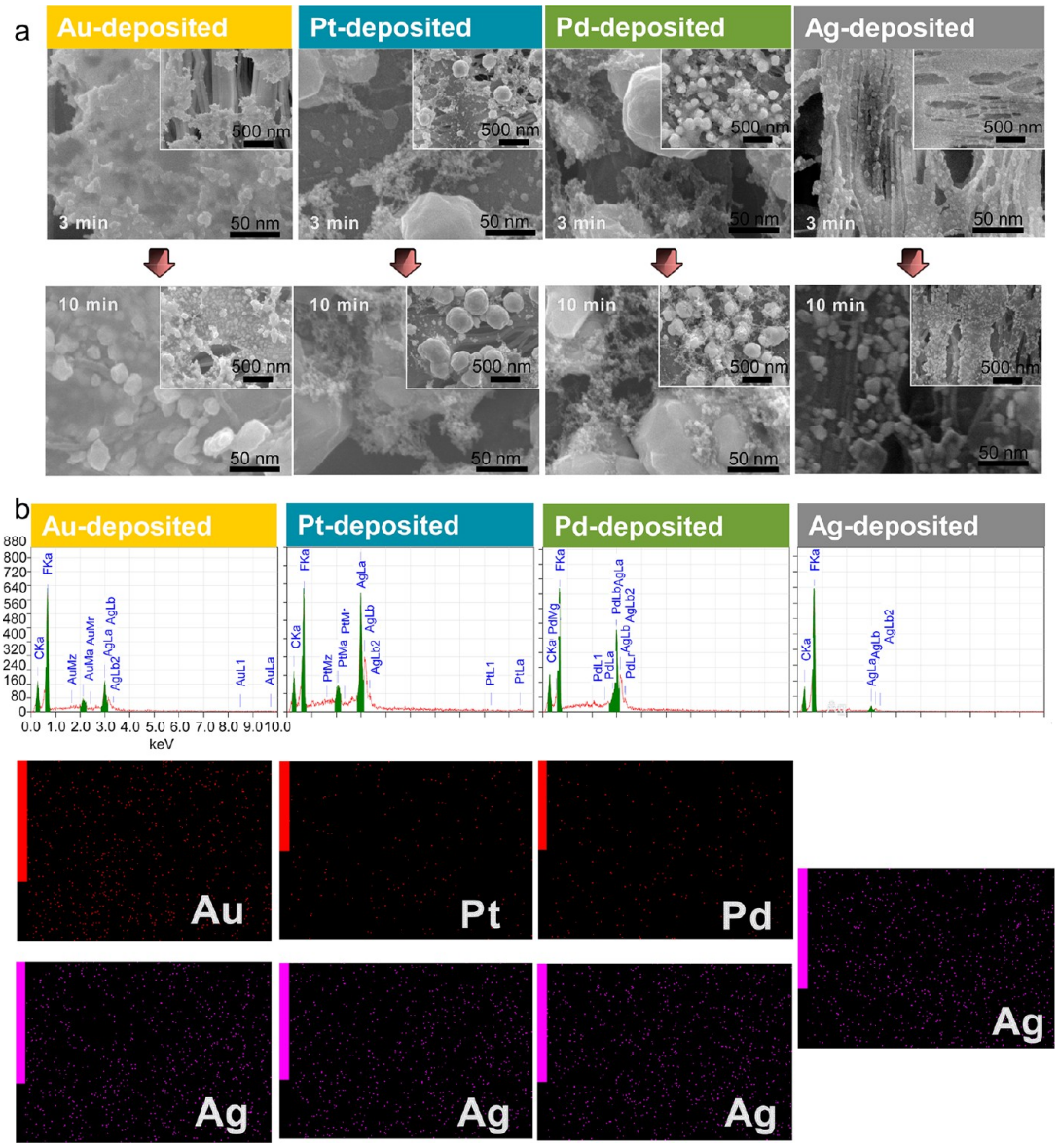

Figure 3. Results of electroless Ag deposition on the activated substrates with the spark-produced particles. (a) Low- and high-magnification SEM images of electroless Ag deposition for 3 and 10 min on the catalytically activated polymer substrates. (b) EDX profiles and maps of the electroless Ag-deposited polymer substrates for 10 min deposition.

and −0.34 V, respectively. The potentials of the Pt nanocatalysts, which could catalyze ELD, were more negative than those of the Au, Pd, and Ag catalysts, which were able to rapidly catalyze ELD. The potentials of the Pt catalysts reached approximately −0.8 V. Thus, it may be concluded that the ELD rate rises as the potential becomes increasingly negative. A representative X-ray diffractometry (XRD, RINT-2100, Rigaku, Japan) profile (inset of Figure 4) shows sharp peaks at around 2θ = 38.2°, 44.4°, 54.5°, and 77.5°. A comparison of these peaks with the data from JCPDS file (No. 01−0783) revealed that these peaks corresponded to the (111), (200), (220), and (311) planes of the fcc phase of Ag, indicating its high crystallinity. A preferred crystal orientation of (111) for all the samples that have undergone a 10 min deposition was evidenced by the XRD results. However, the $I_{(111)}/I_{(200)}$ intensity ratio (∼3.1) for Pt and Pd activated cases was significantly different from the Au and Ag activated ones (∼1.7). Larger spherical Ag particles normally have polycrystalline structures; hence, Ag particles on Pt and Pd catalysts showed relatively smaller $I_{(111)}/I_{(200)}$ ratios. Whereas a nearly identical lattice parameter and a slower Ag deposition may have induced higher $I_{(111)}/I_{(200)}$ ratios.

The obtained bimetallic structures are then employed for catalyzing the conversion of CO. For this reaction, a feed gas of 1% CO in air passed through a 0.04 g catalytic membrane with a total flow rate of 0.067 L min^{-1}, corresponding to a space velocity of ∼1 × 10^5 mL g_{cat}^{-1} h^{-1}. Figure 5 shows the CO conversion versus temperature for bimetallic structures from the Au, Pt, Pd, and Ag nanocatalaysts. At room temperature, pure Ag structures had the lowest activity, and the CO conversion did not reach 100% until the temperature increased to 100 °C, whereas all the bimetallic structures exhibited higher activity than those from pure Ag structures at low temperatures. These results indicate that this enhanced catalytic property should be induced by the synergetic effect of bimetallic structures rather than by the monometallic Ag. This synergy

dx.doi.org/10.1021/am500047n | ACS Appl. Mater. Interfaces 2014, 6, 3105−3110

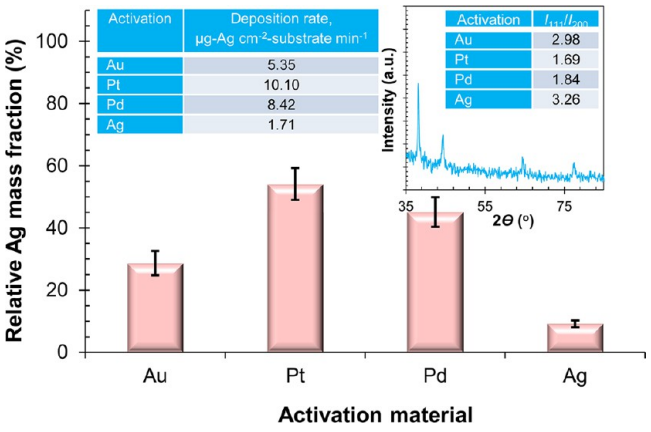

Figure 4. Deposition kinetics of electroless Ag deposition on catalytically activated substrates. Deposition rate of Ag for different aerosol particles is also shown as the inset table. A representative XRD profile, with ratios between I_{111} and I_{200}, is also shown as another inset.

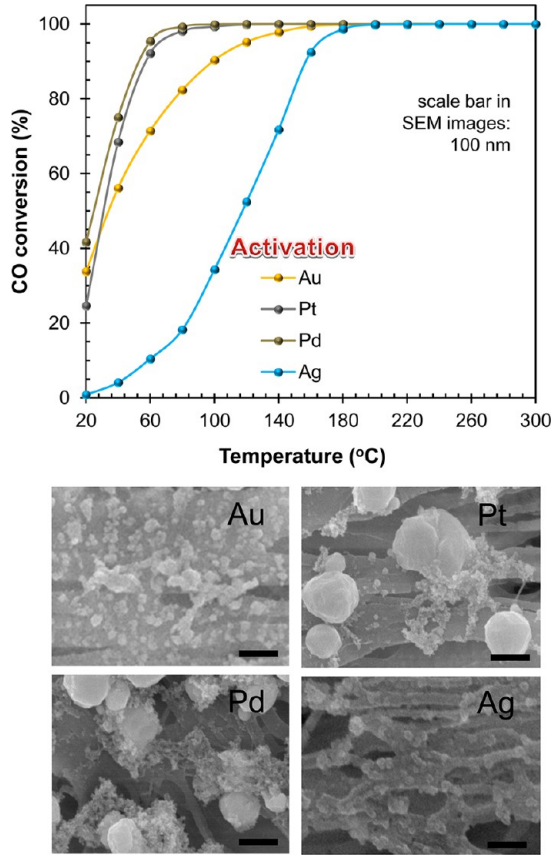

Figure 5. Profiles of CO conversion vs operation temperature with different bimetallic configurations. SEM images of the different configurations after 300 min of CO conversion are also shown in the insets.

most likely occurs when the CO and O_2 are activated in neighboring noble metal and Ag sites on the bimetallic surfaces. The transfer of an oxygen atom between them is thus more easily facilitated. In Figure S3 in the Supporting Information, one can further see that the bimetallic nanostructures gave ~76% conversion at 80 °C with 3% moisture; the CO conversion activity was stable under moist conditions since moisture is one of the major components in practical application environments. We believe the moisture resistance of our membranes may be due to the extremely hydrophobic nature of the PTFE support.

CONCLUSIONS

This work introduced for the first time a comparison in ELD kinetics with different spark-produced noble metal particles to produce bimetallic nanostructures. The fabricated bimetallic structures were further employed as catalysts for efficient CO conversion at low temperature conditions. Due to differences in the catalytic activity of spark-produced nanocatalysts in anodic oxidation of the reducing agent, different Ag deposition kinetics via different hydrazine depletions in the electroless bath were performed in the order of Pt > Pd > Au > Ag. In the case of catalytic CO conversion, due to the synergetic effect of different metals, the as-prepared bimetallic nanostructures showed dramatic higher CO conversion, compared with that of the monometallic Ag catalyst. This strategy may be attractive for various scientific and/or engineering applications for ELD as catalysts and it can also be applied to other fields, such as (opto)electronics, antimicrobial material, and bioanalysis since the aerosol-assisted ELD of substrates is simple, environmentally friendly, and effective (with fewer impurities).

ASSOCIATED CONTENT

Supporting Information

The experimental procedure, mechanism of electroless Ag deposition, morphology and chemistry of untreated substrate, Ag deposition kinetics, electrochemical potentials during silver deposition with different nanocatalysts, CO conversion vs operation time with different bimetallic configurations, and size distributions of spark-produced particles. This material is available free of charge via the Internet at http://pubs.acs.org/.

AUTHOR INFORMATION

Corresponding Authors

*E-mail: jbyeon@purdue.edu. Tel. +1-765-494-5499.
*E-mail: jwkim@hoseo.edu. Tel. +82 41 540 5925. Fax: +82 41 540 5929.

Notes

The authors declare no competing financial interest.

REFERENCES

(1) Quan, Z.; Wang, Y.; Fang, J. High-Index Faceted Noble Metal Nanocrystals. *Acc. Chem. Res.* **2013**, *46*, 191−202.
(2) Sankar, M.; Dimitratos, N.; Miedziak, P. J.; Wells, P. P.; Kiely, C. J.; Hutchings, G. J. Designing Bimetallic Catalysts for a Green and Sustainable Future. *Chem. Soc. Rev.* **2012**, *41*, 8099−8139.
(3) Bosko, M. L.; Marchesini, F. A.; Cornaglia, L. M.; Miró, E. E. *Catal. Commun.* **2011**, *16*, 189−193.
(4) Jang, G. G.; Hawkridge, M. E.; Roper, D. K. Silver Disposition and Dynamics During Electroless Metal Thin Film Synthesis. *J. Mater. Chem.* **2012**, *22*, 21942−21953.
(5) Rebelli, J.; Detwiler, M.; Ma, S.; Williams, C. T.; Monnier, J. R. Synthesis and Characterization of Au−Pd/SiO_2 Bimetallic Catalysts Prepared by Electroless Deposition. *J. Catal.* **2010**, *270*, 224−233.
(6) Lo, S. H.-Y.; Wang, Y.-Y.; Wan, C.-C. Long-Term Stability of Cu/Pd Nanoparticles and Their Feasibility for Electroless Copper Deposition. *Electrochim. Acta* **2008**, *54*, 727−732.
(7) Ye, W.; Li, Y.; Yang, B.; Wang, C. Comparative Study of Electrolessly Deposited Pd/Ag Films onto p-Silicon (100)-Activated Seed Layers of Ag and Pd. *J. Solid State Electrochem.* **2007**, *11*, 1347−1351.

(8) Byeon, J. H.; Ko, B. J.; Hwang, J. Catalytic Activation of Activated Carbon Fibers via Palladium Aerosol Nanoparticles for Use in Electroless Silver Deposition. *J. Phys. Chem. C* **2008**, *112*, 3627−3632.
(9) Fujiwara, Y.; Kobayashi, Y.; Sugaya, T.; Koishikawa, A.; Hoshiyama, Y.; Miyake, H. Adsorption Promotion of Ag Nanoparticle Using Cationic Surfactants and Polyelectrolytes for Electroless Cu Plating Catalysts. *J. Electrochem. Soc.* **2010**, *157*, D211−D216.
(10) Gong, J.; Lipomi, D. J.; Deng, J.; Nie, Z.; Chen, X.; Randall, N. X.; Nair, R.; Whitesides, G. M. Micro- and Nanopatterning of Inorganic and Polymeric Substrates by Indentation Lithography. *Nano Lett.* **2010**, *10*, 2702−2708.
(11) Byeon, J. H.; Kim, J.-W. Site-Selective Catalytic Surface Activation via Aerosol Nanoparticles for Use in Metal Micropatterning. *Langmuir* **2010**, *26*, 11928−11933.
(12) Byeon, J. H.; Kim, J.-W. Carbon Fiber Coating with Silver Using Intervening Au/Pd Nanoparticle Films Produced Using a Spark Discharge. *Thin Solid Films* **2010**, *519*, 700−705.
(13) Byeon, J. H.; Kim, J.-W. Fabrication of a Gold Island Film on Porous Polymeric Substrates by a Strategic Electroless Deposition. *J. Electrochem. Soc.* **2011**, *158*, D15−D20.
(14) Byeon, J. H.; Kim, J.-W. Aerosol Based Fabrication of a Cu/Polymer and Its Application for Electromagnetic Interference Shielding. *Thin Solid Films* **2011**, *520*, 1048−1052.
(15) Tseng, C.-C.; Chang, C.-P.; Sung, Y.; Chen, Y.-C.; Ger, M.-D. A Novel Method to Produce Pd Nanoparticle Ink for Ink-Jet Printing Technology. *Colloids Surf., A* **2009**, *339*, 206−210.
(16) Ayturk, M. E.; Ma, Y. H. Electroless Pd and Ag Deposition Kinetics of the Composite Pd and Pd/Ag Membranes Synthesized from Agitated Plating Baths. *J. Membr. Sci.* **2009**, *330*, 233−245.
(17) Chen, L.; Ma, D.; Zhang, Z.; Guo, Y.; Ye, D.; Huang, B. Synergistic Effect of a Carbon Black Supported PtAg Non-Alloy Bimetal Nanocatalyst for CO Preferential Oxidation in Excess Hydrogen. *ChemCatChem* **2012**, *4*, 1960−1967.
(18) Byeon, J. H.; Kim, Y.-W. Simple Fabrication of a Pd-P Film on a Polymer Membrane and Its Catalytic Applications. *ACS Appl. Mater. Interfaces* **2011**, *3*, 2912−2918.
(19) Shankar, S. S.; Rizzello, L.; Cingolani, R.; Rinaldi, R.; Pompa, P. P. Micro/Nanoscale Patterning of Nanostructured Metal Substrates for Plasmonic Applications. *ACS Nano* **2009**, *3*, 893−900.
(20) Ohno, I.; Wakabayashi, O.; Haruyama, S. Anodic Oxidation of Reductants in Electroless Plating. *J. Electrochem. Soc.* **1985**, *132*, 2323−2330.
(21) Steinbäuser, E. Potential Low-Cost Palladium-Alternatives for Activating Electroless Copper Deposition. *Circuit World* **2010**, *36*, 4−8.
(22) Butler, J. N.; Makrides, A. C. Hydrogen Evolution at Dilute Platinum and Palladium Amalgam Electrodes. *Trans. Faraday Soc.* **1964**, *60*, 938−946.